Observational evidence of diapycnal upwelling within a sloping submarine canyon

Bethan Wynne-Cattanach (bwynneca@ucsd.edu)
University of California, San Diego https://orcid.org/0000-0003-4960-2419

Matthew Alford
https://orcid.org/0000-0002-6318-0737

Nicole Couto
https://orcid.org/0000-0002-5330-9592

Henri Drake
University of California, Irvine

Raffaele Ferrari
Massachusetts Institute of Technology

Arnaud Le Boyer
Scripps Institution of Oceanography

Herle Mercier
IFREMER - Brest https://orcid.org/0000-0002-1940-617X

Marie-Jose Messias
University of Exeter https://orcid.org/0000-0002-3852-2854

Alberto Naveira Garabato
University of Southampton

Kurt Polzin
Woods Hole Oceanographic Institution

Xiaozhou Ruan
Boston University

Carl Spingys
National Oceanography Centre

Hans van Haren
NIOZ Royal Netherlands Insitute for Sea Research and Utrecht University https://orcid.org/0000-0001-8041-8121

Gunnar Voet
University of California, San Diego https://orcid.org/0000-0003-1975-186X

Physical Sciences - Article

Keywords:

Posted Date: October 20th, 2023

DOI: https://doi.org/10.21203/rs.3.rs-3459062/v1

Additional Declarations: There is **NO** Competing Interest.

Observational evidence of diapycnal upwelling within a sloping submarine canyon

Bethan L. Wynne-Cattanach[1], Matthew H. Alford[1], Nicole Couto[1], Henri F. Drake[2], Raffaele Ferrari[3], Arnaud Le Boyer[1], Herlé Mercier[4], Marie-José Messias[5], Alberto Naveira Garabato[6], Kurt Polzin[7], Xiaozhou Ruan[8], Carl P. Spingys[9], Hans van Haren[10], and Gunnar Voet[1]

[1]Scripps Institution of Oceanography, University of California San Diego, La Jolla, CA 92037, USA.

[2]Princeton University / Geophysical Fluid Dynamics Laboratory, Princeton, NJ 08540, USA.

[3]Department of Physical Oceanography, Woods Hole Oceanographic Institution, Woods Hole, MA 02543, USA.

[4]Laboratoire d'Océanographie Physique et Spatiale, CNRS, Ifremer Centre de Bretagne, Plouzané, France.

[5]Deparment of Geography, University of Exeter, Exeter, EX4 4QE, UK.

[6]Ocean and Earth Science, University of Southampton, National Oceanography Centre, Southampton, SO14 3ZH, UK.

[7]Department of Earth, Atmospheric and Planetary Sciences, Massachusetts Institute of Technology, Cambridge, MA 02139, USA

[8]Department of Earth and Environment, Boston University, Boston, MA 02215, USA.

[9]National Oceanography Centre, Southampton, SO14 3ZH, UK.

[10]Royal Netherlands Institute for Sea Research (NIOZ), P.O. Box 59, 1790 AB Den Burg, 30 the Netherlands.

Small-scale turbulent mixing drives the upwelling of deep water masses in the abyssal ocean as part of the global overturning circulation[1]. However, the processes leading to mixing and the pathways through which this upwelling occurs remain insufficiently understood. Recent observational and theoretical work suggests that deep water upwelling may be focused in bottom boundary layers on the ocean's sloping seafloor; however, direct evidence of this is lacking[2;3;4;5]. Here, we present observations from a near-bottom dye release within a canyon on the North Atlantic continental slope showing upwelling across density surfaces at a rate of 250 ± 75 m day^{-1} over three days, ∼10,000 times higher than the global average value required to account for ∼30 Sv of upwelling globally[6]. The vigourous upwelling is coupled with adiabatic exchange of near-boundary and interior fluid. These results provide direct evidence of strong, bottom-focused diapycnal upwelling in the deep ocean, supporting previous suggestions that mixing at topographic features, such as canyons, leads to upwelling[3;7].

The oceanic overturning circulation plays an important role in regulating the global climate by redistributing tracers such as heat, carbon and nutrients throughout the oceans. Transport across density surfaces (isopycnals) by turbulent mixing has long been recognised as a key part of the circulation. Beginning with Munk[6], it has been argued that cross-isopycnal upwelling of deep water is primarily driven by the widespread mixing caused by breaking internal waves in waters deeper than ∼2000 m[5;8;9;10;11]. Tides generate internal wave energy at a rate of ∼1 TW, sufficient to mix abyssal waters across the stable deep stratification to the ocean's ventilated mid-depth and upper layers[8;12;13;14]. Observations in search of the necessary mixing found that turbulent diffusivities in the ocean interior were at least an order of magnitude smaller than the average value needed to close the abyssal buoyancy budget, implying the existence of regions of intense mixing to compensate for the low observations and thus maintain the circulation[15]. More recent measurements have shown that mixing due to breaking internal waves typically intensifies towards the seafloor, particularly around rough topographic features[16;17;18;19;20]. In the ocean interior, a one-dimensional mixing profile integrating these observations (which yields an increase in mixing with depth) implies a divergent turbulent buoyancy flux leading to downwelling[2;3;21]. Thus, internal wave breaking in the interior might not produce the required upwelling as was previously thought, leaving open the question of how deep waters return to the surface.

To resolve this apparent paradox, upwelling may be confined to bottom boundary layers (BBLs)

within which the buoyancy flux perpendicular to the boundary must decrease to zero due to the requirement of no flux through the boundary itself[4;5;22]. The convergent turbulent buoyancy flux leads to upwelling near the boundary. The no flux condition assumes no geothermal heat flux through the seafloor. However, geothermal heat flux reinforces upwelling at the boundary by warming deep waters from below[23;5]. A frictional BBL due to a uniform shear flow above a flat surface is well-mixed and homogeneous. However, above sloping topography, where re-stratification is an important factor and 3-d processes such as internal wave breaking play a role, the definition of a BBL becomes murky.

Microstructure measurements at a Southern Ocean sill[24;25] and within a Mid-Atlantic Ridge fracture zone canyon[3;26] showed enhancement of turbulent dissipation with depth which suggested densification away from the boundary, but lightening along the steep sloping topography. Numerical simulations of deliberate chemical tracer releases showed that the tracer upwelled rapidly as it was advected into the BBL[23;27]. Observations[7;19;28] and subsequent numerical simulations of near-boundary flow[29] suggest a vigorous exchange of mixed fluid with the interior, pointing to the importance of adiabatic and intermittent processes. Together, these results suggest that boundaries may play an important role in upwelling and reinvigorate fundamental debates on the nature of boundary mixing[15;30;31;32]. However, all evidence has, to date, been inferred indirectly from microstructure observations or numerical simulations and based on a range of debatable assumptions.

In this study, we present results from a dye release conducted as part of the Boundary Layer Turbulence and Abyssal Recipes (BLT Recipes) experiment. A major goal of the experiment was to provide observational confirmation of vigorous near-boundary abyssal upwelling, and to explain the physics driving it. The experiment site chosen was the Rockall Trough (Figure 1), given its relatively flat, deep interior and steep sides. These characteristics enable a clear distinction between interior and boundary processes, which is essential for determining the driving forces behind the transformation of deep water. In particular, the study was conducted in a narrow, slope-incising canyon on the eastern side of the Rockall Trough. The canyon is 9 km wide at the mouth and 32 km long from the 2900 m isobath to the tip of the eastern branch of the canyon at the 1200 m isobath. On average, the canyon walls rise 400 m above the thalweg. The canyon splits into a southward and south-eastward branch around 11°W 56' 60", 54°N 13' 48". Our measurements focused on the south-eastward branch of the canyon.

The region has strong barotropic and internal tides that should contribute significantly to mixing on the continental slope[35;36]. The behavior of internal tides interacting with topography depends on the

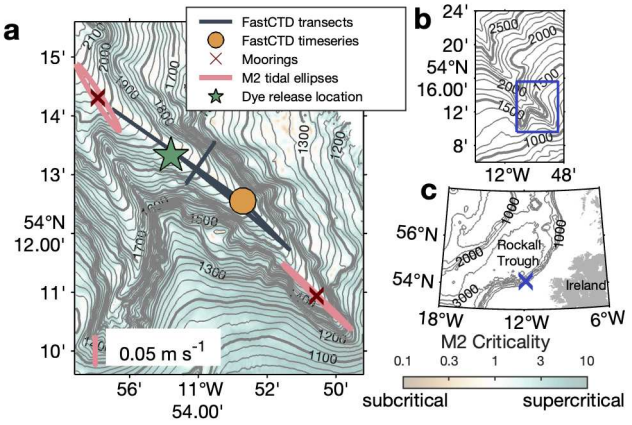

Figure 1: Overview of the study region based on multibeam measurements made during the BLT Recipes experiment and global bathymetry products[33;34]. (a) Canyon bathymetry in the vicinity of the measurements used for this study. Thin contours are every 20 m and thick contours are every 100 m. Locations of the FastCTD transects (black lines), 12 hour time-series station (orange circle), moorings (MP1 and MP2) and dye release are shown. M2 tidal ellipses for each mooring estimated from the average velocity within 100 m of the seafloor are shown with a scale bar of 0.05 m s^{-1}. Shading shows the logarithm of slope criticality to the M2 internal tide given the mean stratification from shipboard CTD stations during the experiment (not shown). (b) Bathymetry of the full canyon. Thin contours are every 100 m, thick contours are every 500 m. The blue box marks the region shown in panel (a). (c) Bathymetry of the Rockall Trough, contours every 1000 m. Land is coloured in grey. The location of the canyon is marked by the blue cross.

ratio of the topographic slope (α) to the propagation angle

$$s = \sqrt{\frac{\omega^2 - f^2}{N^2 - \omega^2}} \tag{1}$$

of the internal wave (the criticality)[37], where ω is the internal wave frequency, f is the local inertial frequency and N^2 is the buoyancy frequency. To estimate criticality, we use the time-mean buoyancy frequency estimated from shipboard CTD casts collected within and around the canyon during the BLT Recipes experiment. The canyon thalweg, with an average slope of 4°, has a similar slope to the internal semi-diurnal (M2) tides ($\frac{\alpha}{s} \approx 1$), implying local generation and critical reflection of the internal tide within the canyon. The canyon side walls are supercritical ($\frac{\alpha}{s} > 1$; blue colours in Figure 1), which tends to lead to reflection and scattering of incident waves.

Time series from a short-term mooring (MP1) deployed near the canyon fork document flow primarily parallel to the axis of the canyon, with flow reversals occurring twice daily. Daily asymmetry in peak velocity strength indicates the presence of both a semi-diurnal and diurnal internal tide (Figure 2). Note that the diurnal tide is topographically trapped at this location as the diurnal frequency is sub-inertial.

Up-canyon flow brings dense water up from deeper in the canyon, while isopycnals plunge downward during down-canyon flow.

Diapycnal upwelling measured by dye

To directly measure the diapycnal transformation of deep water in the canyon, a cloud of fluorescein dye was released near the seafloor in the centre of the canyon. Previous dye releases have focused on shallow, coastal or lake environments[38;39;40;41;42]. Here, the dye was released in 1870 m of water, approximately 10 m above the canyon floor and at a conservative temperature of 3.53 °C. The rapid profiling "Fast CTD" (FCTD; details in Methods) carried a fluorometer, enabling high spatial and temporal resolution profiles of dye down to 2200 m depth and facilitating direct observations of the effect of turbulent mixing near the sloping bottom. Also onboard the FCTD was a micro-conductivity probe that measured the dissipation rate of temperature variance (χ), a measure of effective turbulent mixing. We focus on transformation of the dye within the first 3 days after release.

The dye allows us to quantify the rate of flow across isopycnals, or equivalently the lightening rate needed to keep the system in steady state. To do this, we track the evolution of the dye in density space using the dye weighted average[43;44] (see Methods). We use the density variable of potential density anomaly, $\sigma_\theta = \rho_\theta - 1000$ kg m^{-3}, referenced to a pressure of 1500 db. While seawater density depends on both temperature and salinity, density is approximately linear in temperature in this region[45], permitting us to use temperature and density interchangeably to characterize upwelling.

The first moment of potential density anomaly, $\overline{\sigma_\theta}$, estimated using the tracer-weighted average, represents the centre of mass of the dye in density space. By estimating how the density of dyed waters decreased with time we can infer an upwelling rate across isopycnals (Figure A4). The first observation of the dye was made two hours after release (Figure 3a). The dye cloud was still very concentrated at this time. The centre of mass was at a potential density anomaly of $\sigma_\theta = 34.660$ kg m^{-3}. Little mixing with lighter waters occurred since the dye release at $\sigma_\theta = 34.661$ kg m^{-3} (Figure 3d). The isotherms were stretched vertically, indicative of a large overturning event due to internal wave breaking on the slope. Vigorous turbulent mixing was seen along the upper edge of the bore, over 100 m above the seafloor (pink contour, Figure 3a). The dye likely mixed strongly across this interface. Fifteen hours after release, the dye was observed as the ship travelled down the canyon (Figure 3b). The dye had lightened since the

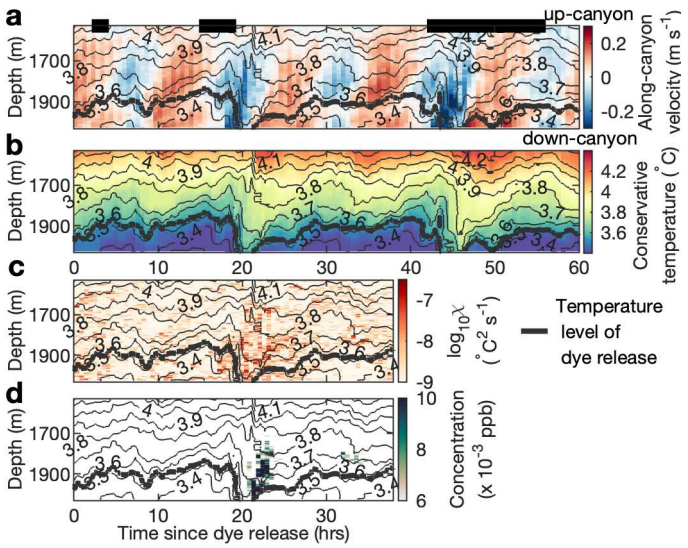

Figure 2: Moored measurements of (a) along-canyon velocity (up-canyon is positive), (b) conservative temperature, (c) dissipation rate of temperature variance on a log scale and (d) dye concentration in parts per billion from MP1. The threshold for dye concentration detection for the fluorometer onboard the MP1 is 0.006 ppb. Thin black contours show every 0.1 °C. The release isotherm of 3.53 °C in conservative temperature is shown with the thick black contour. Thick black lines along the top of panel (a) indicate times of FCTD transects shown in Figure 3. Note that the battery for dissipation and fluorometer measurements stopped around 38 hours after the dye release.

up-canyon transect, and the centre of mass was at $\sigma_\theta = 34.632$ kg m^{-3}. Less turbulence was observed during this transect, consistent with other observations that mixing is associated with up-canyon tidal flow[19;46;45]. Note that in contrast, mixing at MP1, further down the canyon, is associated with down-canyon flow. Over the subsequent observations, the dye became more diffuse and spread both vertically and horizontally, as seen during the FCTD time series completed at the end of the survey (Figure 3c).

Using a weighted linear regression to the observed centres of mass (see Methods), we observed a diapycnal upwelling rate (w_{dye}) of 250 ± 75 m day^{-1} over all observations. Velocity measurements from both the MP1 (1 week record) and MP2 (3 month record) moorings show that the record-mean along-canyon flow was up-canyon within 500 m of the seafloor and density decreased towards the head of the canyon (Figure 4). The momentum balance driving the up-canyon flow is currently under investigation. Candidate driving forces include i) large-scale pressure gradients set by the mesoscale and/or mean circulation fields and ii) convergent radiation stresses[47]. Regardless, the flow is constricted by the canyon topography, so in order to maintain this along-canyon flow down the density gradient, there must be mixing across isopycnals[21;48;49]. Since the canyon is sloping upwards, the flow must have a vertical component $u_{along} \sin\alpha$ where u_{along} is along-canyon velocity and α is the bathymetric slope.

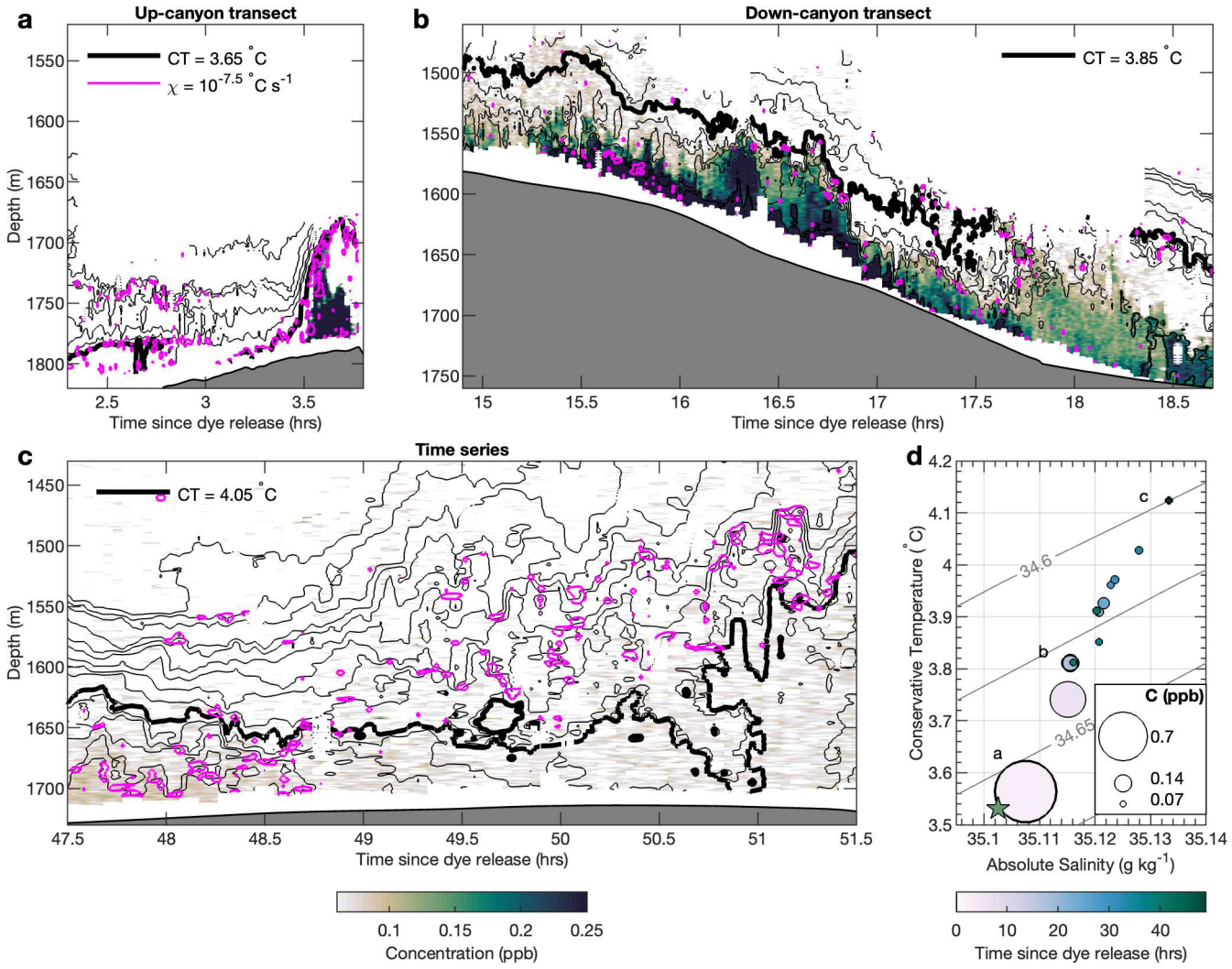

Figure 3: Example observations of dye concentration measured using the FCTD at (a) 2.5 hours, (b) 15 hours and (c) 47.5 hours after release. Dye concentration is shown in parts per billion (ppb) in colour, isotherms who's mean depths are separated by 10 m are shown with thin black contours and the $\chi = 1 \times 10^{-7.5}$ °C^{2}s^{-1} contour is shown in magenta on each panel denoting regions of enhanced turbulent mixing. Thick black contours indicate reference conservative temperatures 3.65 °C, 3.85 °C and 4.05 °C for panels (a), (b) and (c) respectively. The threshold of dye concentration detection for the fluorometer onboard the FCTD is 0.06 ppb. Panel (d) shows a temperature-salinity diagram of the centre of mass for each transect. Scatter points are coloured by time since the dye release in hours and the size of the data point indicates average concentration during the transect. Scatters with thick outlines are labelled a, b and c, and correspond to the examples shown in panels (a), (b) and (c). Temperature and salinity at which the dye was released is marked with the green star. Grey contours show lines of constant potential density anomaly in kg m^{-3}. (See Figure A5 for the full temperature-salinity distribution of each transect.)

Using the time and depth mean along-canyon velocity of 0.02 m s^{-1} from the week-long MP1 record leads to a mean vertical upwelling velocity of ∼100 m day^{-1}. Our estimate of the upwelling velocity from the observed velocities is consistent to within a factor of 2.5 of the dye-inferred value, giving confidence in our result.

Exchange with the interior

The MP1 mooring was located down-canyon of the release site during the dye experiment. The dye reached the mooring twice, 20 hours after release and 32 hours after release (Figure 2). The FCTD survey of the dye 20 hours after release (Figure 4) captured the up-canyon edge of the dye. Dye concentrations were much lower at the mooring than at the FCTD location, suggesting that only the edge of the patch reached the mooring location. These two sets of measurements suggest that the patch size 20 hours after release was at least 4 km in length (note that the fluorometer on the mooring was 10 times more sensitive than the one on the FCTD (see methods), therefore, additional weakly concentrated dye further up the canyon may have gone undetected by the FCTD). In both the FCTD and mooring record the dye was colder than the 3.85 °C isotherm. In the mooring record, the dye remained warmer than the release isotherm suggests the dye was confined between the 3.53 °C and 3.85 °C isotherms along the canyon. The dye was ∼50 m at MP1, forming a tongue of dye that extended into the interior. Given the along-canyon tidal excursion ∼ 4 km this picture is consistent with periodic advection of dye into the interior by tidal sloshing[29].

Summary

This work provides direct evidence of diapycnal upwelling along a sloping canyon in the deep ocean. Upwelling velocities of 250 ± 75 m day^{-1} unambiguously demonstrate that processes at steeply sloping topography led to rapid upwelling of deep water to lighter density classes.

Diapycnal upwelling observed here is four orders of magnitude larger than the average upwelling value inferred from the ocean interior required to maintain the global deep-ocean density stratification[6]. In a fracture zone canyon of the Mid-Atlantic Ridge, the mean upwelling velocity inferred from along-canyon velocity was 1.7 m day^{-1} [26]. Up-canyon velocity magnitude was similar to that seen here,

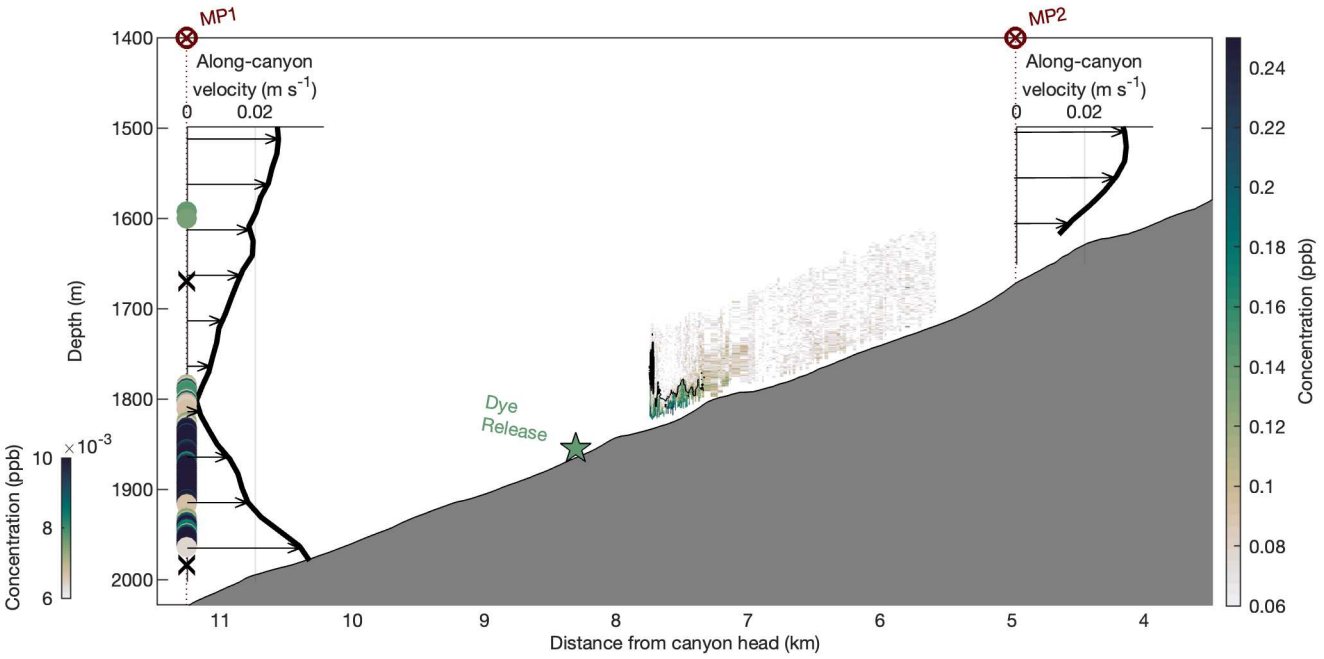

Figure 4: Along-canyon overview of the observations, in distance from the head of the canyon (see Figure A2 for a map showing along-canyon distances). Inset axes show time mean profiles of along-canyon velocity at MP1 (located at 11.3 km along the canyon, averaged over the full 1-week record) and MP2 (located at 4.8 km along the canyon, averaged over the full 3-month record. Note that MP2 was deployed after MP1 was taken out of the water). Dye concentration from an example transect 20 hours after the dye release along the canyon axis is shown between 5.5 and 8 km, with the highest concentrations shown with green colours (see Figure A1d for more detail). The 3.85°C isotherm is contoured in black. Coloured dots show dye concentration measured using the fluorometer on the MP1 mooring also at 20 hours after release. Note that colour scales for dye transect and moored profile dye concentrations are different and the detection threshold is 0.06 ppb for the FCTD measurements and 0.006 ppb for the MP1 measurement. Depths of the 3.85 °C and 3.53 °C isotherms at this time are marked with black crosses on the MP1 profile.

however, the much shallower bathymetric slope led to a relatively smaller upwelling velocity. Diapycnal upwelling in the Mid-Atlantic Ridge canyon has been determined to be controlled by the shape of the topography (hypsometry)[26;32]. In Monterey Canyon, estimates of upwelling using microstructure turbulence observations were also up to 3 orders of magnitude smaller than our observations and ranged from 0.2 to 1 m day^{-1} over the BBL due to hypsometry. The hypsometry of our canyon is insufficient to produce the observed upwelling (see Methods). Global estimates of diapycnal velocities based on a parametrisation of tidal mixing yield boundary-focused upwelling velocities up to $\sim 1 \times 10^{-3}$ m day^{-1} in the abyssal ocean[50]. Differences between the 0.5° resolution bathymetry used and local topography may lead to lower turbulence values than are required to give the upwelling observed here. The tidal mixing climatology also does not account for the spring-neap cycle or time-variability in stratification[51].

While observational limitations in this study lead to uncertainty in the dye-inferred upwelling actually experienced by the dye the similarity between independent estimates of dye-based upwelling and diapycnal upwelling due to along-canyon flow is encouraging.

Diapycnal upwelling was coupled with tidal sloshing that transported dye away from the boundary along isopycnals. Complementary observations from the FTCD and long-term moorings during our experiment found that periods of intense mixing and upwelling were associated with convective breaking of the internal tide within the canyon[45] (A.C.N.G., C.P.S., M.H.A., Bieto Fernández-Castro, K.L.P., G.V., B.L.W.C., N.C., Alexander Forryan, H.F.D., X.R., H.M., M.J.M., Eleanor E. Frajka-Williams, R.F. (in prep.)). Episodic internal wave breaking has been observed elsewhere, on steep slopes within canyons[46;52;53], on seamounts[19], ridges[54;55] and continental shelves[56;57]; however, the shear or convective nature of the breaking varies by location. Our results provide support for previous theoretical and numerical studies which propose that near-boundary mixing is important for deep-ocean upwelling[4;5;22;27]. However, these previous studies focused on diabatic and steady flows, unlike the tidally modulated flows we observed here.

Our work suggests that acknowledgement of the time-variable, three-dimensional nature of near-boundary mixing processes may be essential to the adequate representation and understanding of BBL upwelling physics. Based on our observations and the widespread distribution of submarine canyons across the globe, previous global scalings based on weaker upwelling velocities may be underestimates[26;7;50]. Upwelling within these canyons may play an even more significantly role in the upwelling of deep-water than previously thought.

References

[1] Wunsch, C. and Ferrari, R. Vertical Mixing, Energy and the General Circulation of the Oceans. *Ann. Rev. Fluid Mech.*, 36:281–314, 2004. doi: 10.1146/annurev.fluid.36.050802.122121.

[2] Ledwell, J. R., Montgomery, E. T., Polzin, K. L., Laurent, L. C. S., Schmitt, R. W., and Toole, J. M. Evidence for enhanced mixing over rough topography in the abyssal ocean. *Nature*, 403: 179–182, 2000. doi: 10.1038/35003164.

[3] St. Laurent, L., Toole, J. M., and Schmitt, R. W. Buoyancy Forcing by Turbulence above Rough Topography in the Abyssal Brazil Basin. *J. Phys. Oceanogr.*, 31:3476–3495, 2001. doi: 10.1175/1520-0485(2001)031%3C3476:BFBTAR%3E2.0.CO;2.

[4] Ferrari, R., Mashayek, A., McDougall, T. J., Nikurashin, M., and Campin, J. M. Turning ocean mixing upside down. *J. Phys. Oceanogr.*, 46(7):2239–2261, July 2016. ISSN 15200485. doi: 10.1175/JPO-D-15-0244.1.

[5] De Lavergne, C., Madec, G., Le Sommer, J., Nurser, A. G., and Naveira Garabato, A. C. On the consumption of Antarctic Bottom Water in the abyssal ocean. *J. Phys. Oceanogr.*, 46(2):635–661, 2016. doi: 10.1175/JPO-D-14-0201.1.

[6] Munk, W. H. Abyssal recipes. *Deep-Sea Res. Oceanogr. Abstr.*, 13(4):707–730, 1966. ISSN 0011-7471. doi: 10.1016/0011-7471(66)90602-4.

[7] Kunze, E., MacKay, C., McPhee-Shaw, E. E., Morrice, K., Girton, J. B., and Terker, S. R. Turbulent Mixing and Exchange with Interior Waters on Sloping Boundaries. *J. Phys. Oceanogr.*, 42(6):910–927, June 2012. ISSN 0022-3670. doi: 10.1175/JPO-D-11-075.1.

[8] Munk, W. H. and Wunsch, C. Abyssal Recipes II: Energetics of tidal and wind mixing. *Deep Sea Res. Part I Oceanogr. Res. Pap.*, 45:1977–2010, 1998. doi: 10.1016/S0967-0637(98)00070-3.

[9] Lumpkin, R. and Speer, K. Global Ocean Meridional Overturning. *J. Phys. Oceanogr.*, 37:2550–2562, 2007. doi: 10.1175/JPO3130.1.

[10] Talley, L. D. Closure of the global overturning circulation through the Indian, Pacific, and Southern Oceans: Schematics and transports. *Oceanography*, 26(1):80–97, 2013.

[11] Ferrari, R. Oceanography: What goes down must come up. *Nature*, 513:179–180, 2014. ISSN 0028-0836. doi: 10.1038/513179a.

[12] Egbert, G. D. and Ray, R. D. Significant dissipation of tidal energy in the deep ocean inferred from satellite altimeter data. *Nature*, 405(6788):775–778, 2000. doi: 10.1038/35015531.

[13] Nycander, J. Generation of internal waves in the deep ocean by tides. *J. Geophys. Res. Oceans*, 110(C10), 2005. doi: 10.1029/2004JC002487.

[14] Garrett, C. and Kunze, E. Internal Tide Generation in the Deep Ocean. *Annu. Rev. Fluid Mech.*, 39(1):57–87, January 2007. ISSN 0066-4189. doi: 10.1146/annurev.fluid.39.050905.110227.

[15] Garrett, C. Comment on 'Some evidence for boundary mixing in the deep ocean'. *J. Geophys. Res.*, 84:5095, 1979. doi: 10.1029/JC084iC08p05095.

[16] Gargett, A. E. Vertical eddy diffusivity in the ocean interior. *J. Mar. Res.*, pages 359–393, 1984. doi: 10.1357/002224084788502756.

[17] Polzin, K. L., Toole, J. M., Ledwell, J. R., and Schmitt, R. W. Spatial variability of turbulent mixing in the abyssal ocean. *Science*, 276:93–96, 1997. doi: 10.1126/science.276.5309.93.

[18] Rudnick, D. L., Boyd, T. J., Brainard, R. E., Carter, G. S., Egbert, G. D., Gregg, M. C., Holloway, P. E., Klymak, J. M., Kunze, E., Lee, C. M., et al. From tides to mixing along the Hawaiian Ridge. *science*, 301(5631):355–357, 2003.

[19] van Haren, H. and Gostiaux, L. Detailed internal wave mixing above a deep-ocean slope. *J. Mar. Res.*, 70(1):173–197, 2012. doi: 10.1357/002224012800502363.

[20] Waterhouse, A. F., MacKinnon, J. A., Nash, J. D., Alford, M. H., Kunze, E., Simmons, H. L., Polzin, K. L., St. Laurent, L. C., Sun, O. M., Pinkel, R., Talley, L. D., Whalen, C. B., Huussen, T. N., Carter, G. S., Fer, I., Waterman, S., Naveira Garabato, A. C., Sanford, T. B., and Lee, C. M. Global Patterns of Diapycnal Mixing from Measurements of the Turbulent Dissipation Rate. *J. Phys. Oceanogr.*, 44(7):1854–1872, July 2014. ISSN 0022-3670. doi: 10.1175/JPO-D-13-0104.1.

[21] Thurnherr, A. M., Laurent, L. C. S., Speer, K. G., Toole, J. M., and Ledwell, J. R. Mixing Associated with Sills in a Canyon on the Midocean Ridge Flank. *J. Phys. Oceanogr.*, 35:1370–1381, 2005. doi: 10.1175/JPO2773.1.

[22] McDougall, T. J. and Ferrari, R. Abyssal Upwelling and Downwelling Driven by Near-Boundary Mixing. *J. Phys. Oceanogr.*, 47(2):261–283, 2017. doi: 10.1175/JPO-D-16-0082.1.

[23] Mashayek, A., Ferrari, R., Merrifield, S., Ledwell, J. R., St Laurent, L., and Garabato, A. N. Topographic enhancement of vertical turbulent mixing in the Southern Ocean. *Nat. Commun.*, 8 (1):14197, April 2017. ISSN 2041-1723. doi: 10.1038/ncomms14197.

[24] Naveira Garabato, A. C., Frajka-Williams, E. E., Spingys, C. P., Legg, S., Polzin, K. L., Forryan, A., Abrahamsen, E. P., Buckingham, C. E., Griffies, S. M., McPhail, S. D., Nicholls, K. W., Thomas, L. N., and Meredith, M. P. Rapid mixing and exchange of deep-ocean waters in an abyssal boundary current. *Proc. Natl. Acad. Sci.*, 116(27):13233–13238, 2019. doi: 10.1073/pnas.1904087116.

[25] Spingys, C. P., Garabato, A. C. N., Legg, S., Polzin, K. L., Abrahamsen, E. P., Buckingham, C. E., Forryan, A., and Frajka-Williams, E. E. Mixing and Transformation in a Deep Western Boundary Current: A Case Study. *J. Phys. Oceanog.*, 51(4):1205–1222, 2021. doi: 10.1175/JPO-D-20-0132.1.

[26] Thurnherr, A. M., Clément, L., St. Laurent, L., Ferrari, R., and Ijichi, T. Transformation and Upwelling of Bottom Water in Fracture Zone Valleys. *J. Phys. Oceanogr.*, 50(3):715–726, 2020. doi: 10.1175/JPO-D-19-0021.1.

[27] Drake, H. F., Ruan, X., and Ferrari, R. Diapycnal Displacement, Diffusion, and Distortion of Tracers in the Ocean. *J. Phys. Oceanogr.*, 52(12):3221–3240, 2022. doi: 10.1175/JPO-D-22-0010.1.

[28] van Haren, H. Nonlinear motions at the internal tide source. *Geophys. Res. Lett.*, 33(11), 2006. doi: 10.1029/2006GL025851.

[29] Winters, K. B. Tidally driven mixing and dissipation in the stratified boundary layer above steep submarine topography. *Geophys. Res. Lett.*, 42(17):7123–7130, September 2015. ISSN 19448007. doi: 10.1002/2015GL064676.

[30] Armi, L. Some evidence for boundary mixing in the deep ocean. *J. Geophys. Res.*, 83(C4):1971–1979, 1978. doi: 10.1029/JC083iC04p01971.

[31] Garrett, C. An Isopycnal View of Near-Boundary Mixing and Associated Flows. *J. Phys. Oceanogr.*, 31(1):138–142, 2001. doi: 10.1175/1520-0485(2001)031<0138:AIVONB>2.0.CO;2.

[32] Polzin, K. L. and McDougall, T. J. Chapter 7 - Mixing at the ocean's bottom boundary. In Meredith, M. and Garabato, A. N., editors, *Ocean Mixing*, pages 145–180. Elsevier, New York, U.S.A., 2022. ISBN 978-0-12-821512-8. doi: 10.1016/B978-0-12-821512-8.00014-1.

[33] GEBCO Compilation Group. GEBCO 2023 Grid, 2023.

[34] Smith, W. H. and Sandwell, D. T. Global sea floor topography from satellite altimetry and ship depth soundings. *Science*, 277(5334):1956–1962, 1997.

[35] Huthnance, J. M. The Rockall slope current and shelf-edge processes. *Proc. R. Soc. B: Biol. Sci.*, 88:83–101, 1986. doi: 10.1017/S0269727000004486.

[36] Sherwin, T. J. and Taylor, N. K. Numerical investigations of linear internal tide generation in the Rockall Trough. *Deep Sea Res. Part I Oceanogr. Res. Pap.*, 37(10):1595–1618, 1990. ISSN 0198-0149. doi: 10.1016/0198-0149(90)90064-3.

[37] LeBlond, P. H. and Mysak, L. A. *Waves in the Ocean*. Elsevier, New York, U.S.A., 1981.

[38] Ledwell, J. R., Duda, T. F., Sundermeyer, M. A., and Seim, H. E. Mixing in a coastal environment: 1. A view from dye dispersion. *J. Geophys. Res. Oceans*, 109(C10), 2004. doi: 10.1029/2003JC002194.

[39] Sundermeyer, M. A., Terray, E. A., Ledwell, J. R., Cunningham, A. G., LaRocque, P. E., Banic, J., and Lillycrop, W. J. Three-Dimensional Mapping of Fluorescent Dye Using a Scanning, Depth-Resolving Airborne Lidar. *J. Atmos. Ocean. Tech.*, 24(6):1050–1065, 2007. doi: 10.1175/JTECH2027.1.

[40] Wain, D. J. and Rehmann, C. R. Transport by an intrusion generated by boundary mixing in a lake. *Water Resour. Res.*, 46(8), 2010. ISSN 1944-7973. doi: 10.1029/2009WR008391.

[41] Clark, D. B., Lenain, L., Feddersen, F., Boss, E., and Guza, R. T. Aerial Imaging of Fluorescent Dye in the Near Shore. *J. Atmos. Ocean. Tech.*, 31(6):1410–1421, 2014. doi: 10.1175/JTECH-D-13-00230.1.

[42] Johansen, K., Dunne, A. F., Tu, Y.-H., Almashharawi, S., Jones, B. H., and McCabe, M. F. Dye tracing and concentration mapping in coastal waters using unmanned aerial vehicles. *Scientific Reports*, 12(1):1141, January 2022. ISSN 2045-2322. doi: 10.1038/s41598-022-05189-9.

[43] Holmes, R. M., de Lavergne, C., and McDougall, T. J. Tracer transport within abyssal mixing layers. *J. Phys. Oceanogr.*, 49(10):2669–2695, 2019. doi: 10.1175/JPO-D-19-0006.1.

[44] Ruan, X. and Ferrari, R. Diagnosing Diapycnal Mixing from Passive Tracers. *J. Phys. Oceanog.*, 51(3):757–767, March 2021. ISSN 0022-3670. doi: 10.1175/JPO-D-20-0194.1.

[45] van Haren, H., Voet, G., Alford, M. H., Fernández-Castro, B., Garabato, A. C. N., Wynne-Cattanach, B. L., Mercier, H., and Messias, M.-J. Near-slope turbulence in a Rockall canyon. *Deep Sea Res. Part I Oceanogr. Res. Pap.*, submitted.

[46] van Haren, H., Mienis, F., and Duineveld, G. Contrasting internal tide turbulence in a tributary of the Whittard Canyon. *Cont. Shelf Res.*, 236:104679, 2022. doi: 10.1016/j.csr.2022.104679.

[47] Marques, O. B. *From Large-Scale Internal Tides to Small-Scale Turbulence: Observations on the Continental Slope off Tasmania*. PhD thesis, UC San Diego, 2021.

[48] Ruan, X. and Callies, J. Mixing-driven mean flows and submesoscale eddies over mid-ocean ridge flanks and fracture zone canyons. *J. Phys. Oceanogr.*, 50(1):175–195, 2020. doi: 10.1175/JPO-D-19-0174.1.

[49] Peterson, H. G. and Callies, J. Rapid spinup and spindown of flow along slopes. *J. Phys. Oceanogr.*, 52(4):579–596, 2022. doi: 10.1175/JPO-D-21-0173.1.

[50] Cimoli, L., Mashayek, A., Johnson, H. L., Marshall, D. P., Naveira Garabato, A. C., Whalen, C. B., Vic, C., de Lavergne, C., Alford, M. H., MacKinnon, J. A., et al. Significance of diapycnal mixing within the Atlantic Meridional Overturning Circulation. *AGU adv.*, 4(2):e2022AV000800, 2023. doi: 10.1029/2022AV000800.

[51] de Lavergne, C., Vic, C., Madec, G., Roquet, F., Waterhouse, A. F., Whalen, CB., Cuypers, Y., Bouruet-Aubertot, P., Ferron, B., and Hibiya, T. A parameterization of local and remote tidal mixing. *J. Adv. Model. Earth Syst.*, 12(5):e2020MS002065, 2020. doi: 10.1029/2020MS002065.

[52] Alberty, M. S., Billheimer, S., Hamann, M. M., Ou, C. Y., Tamsitt, V., Lucas, A. J., and Alford, M. H. A reflecting, steepening, and breaking internal tide in a submarine canyon. *J. Geophys. Res. Oceans*, 122:6872–6882, 2017. doi: 10.1002/2016JC012583.

[53] Lee, I.-H., Lien, R.-C., Liu, J. T., and Chuang, W. Turbulent mixing and internal tides in Gaoping (Kaoping) Submarine Canyon, Taiwan. *J. Mar. Syst.*, 76:383–396, 2009. doi: 10.1016/j.jmarsys.2007.08.005.

[54] Aucan, J., Merrifield, M. A., Luther, D. S., and Flament, P. Tidal Mixing Events on the Deep Flanks of Kaena Ridge, Hawaii. *J. Phys. Oceanogr.*, 36(6):1202–1219, June 2006. ISSN 1520-0485, 0022-3670. doi: 10.1175/JPO2888.1.

[55] Levine, M. D. and Boyd, T. J. Tidally Forced Internal Waves and Overturns Observed on a Slope: Results from HOME. *J. Phys. Oceanogr.*, 36(6):1184–1201, June 2006. ISSN 1520-0485, 0022-3670. doi: 10.1175/JPO2887.1.

[56] Klymak, J. M., Alford, M. H., Pinkel, R., Lien, R. C., and Yang, Y. J. The breaking and scattering of the internal tide on a continental slope. *J. Phys. Oceanogr.*, 41(5):926–945, 2011. doi: 10.1175/2010JPO4500.1.

[57] Nash, J. D., Alford, M. H., Kunze, E., Martini, K., and Kelly, S. Hotspots of deep ocean mixing on the Oregon continental slope. *Geophys. Res. Lett.*, 34(1):L01605, January 2007. ISSN 0094-8276. doi: 10.1029/2006GL028170.

Methods

BLT Recipes Experiment

The data presented here were collected during expedition DY132 of *RRS Discovery*[1] between June 19, 2021 and July 29, 2021, supported by the NERC and NSF-funded Boundary Layer Turbulence and Abyssal Recipes project. The experiment consisted of a dye release together with surveys and moorings measuring hydrographic data, velocity, and shear and temperature microstructure.

Dye release

A fluorescent dye (fluorescein $C_{20}H_{10}O_5Na_2$) was used for this experiment. The mixture used for the release consisted of 64 L of isopropyl, 6 L of seawater and 149 L of 40% fluorescein liquid. The mixture was chosen to be denser than the local water at the desired depth to ensure that it was released properly and did not rise without mixing. The dye release system (InkBot) comprises a 219 L drum equipped with a Seabird SBE 911plus CTD, an AQUAtracka III fluorometer (Chelsea Technologies Group), an altimeter, and an OCEANO 2500S Universal acoustic release. For deployment, the InkBot was attached to the CTD sea cable and lowered to 10 m above the bottom using the ship winch. Once in position, the drum was emptied by simultaneously flipping the drum and opening the drum lid using the acoustic release. The drum was upside down for 15 minutes, while readings from the onboard CTD enabled the winch operator to ensure that the InkBot remained at the release temperature. The dye release began at 03:01 am on July 1, 2021. The dye release surveys were completed using the Fast CTD.

Fast CTD

The Fast CTD (FCTD) system[2] is a tethered profiler with a Seabird SBE49 CTD, a dual needle micro-conductivity probe (built in-house at Scripps Institution of Oceanography by the Multiscale Ocean Dynamics group) and for this experiment, a Turner C-FLUOR fluorometer and an altimeter. The instrument was raised and lowered with a direct drive electric winch at vertical speeds of approximately $3\,\mathrm{m\ s^{-1}}$ while the ship was steaming at a speed of 0.5–1 knot. Data from both up and down-casts were used. The goal of the FCTD survey was to sample the dye release as many times as possible before dye concentrations became too low to be detected. Transects were focused along the canyon axis to transit from one end of the dye patch to the other before turning around and repeating. Additionally, two cross-canyon transects and a 12 hour time-series station were completed to better understand the full extent of the dye patch. During a transect, the FCTD profiled over $\sim$100 m vertical range and to within < 10 m of the seafloor. Data from the FCTD were monitored and used interactively to guide the survey.

The micro-conductivity probe was used to estimate dissipation rate of temperature variance (χ). Conductivity gradients can be used since temperature dominates the conductivity variance[3].

MP1 Mooring

The mooring (MP1) was deployed on the canyon axis at 2028-m water depth. The mooring was 600 m tall and consisted of a downward looking RDI Longranger 75 kHz Acoustic Doppler Current Profiler (ADCP) mounted in the top float and a McLane Moored Profiler outfitted with a Seabird SBE52 CTD, a Falmouth Scientific Inc acoustic current meter, and an Epsilometer turbulence package (Multiscale Ocean Dynamics group, Scripps Institution of Oceanography)[4] to measure χ from temperature gradients, and a Turner C-FLUOR fluorometer. The profiler was deployed on June 28, 2021, and profiled continuously for 7 days, collecting one profile every 30 minutes.

Fluorometer calibration

The Turner C-FLUOR fluorometer calibration uses the linear relationship $C = (V - a)b$ where C is the concentration in parts per billion, V the measured voltage, a an offset and b the calibration coefficient. The offset voltage was lower than the factory-provided value for both fluorometers used. For MP1, we used profiles before the dye release, and for the FCTD we used the upper 500 m of down-casts from the surface to measure the mean background voltage when zero dye was present. We used the factory calibration coefficient for both fluorometers. This gave calibrations of $C_{FCTD} = (V_{FCTD} - 0.0140) * 31.1831$ and $C_{MP} = (V_{MP} - 0.0139) * 31.3309$. The minimum detectable level of the fluorometers was determined as three standard deviations above the mean background level. This gave minimum detectable concentrations of 0.06 ppb for the fluorometer on the FCTD and 0.006 ppb for the fluorometer on MP1. The factor of 10 difference between detection limits is likely due to individual sensor differences and an electrically noisier channel on the FCTD. Observed dye concentrations at MP1 were up to three times the detection limit. At the end of the FCTD survey, the levels were down to twice the detection limit.

Sampling uncertainty

Due to high flow speeds, up to 0.4 m s^{-1} along the canyon, the dye was advected rapidly along the canyon, requiring the dye survey to focus on two-dimensional transects through the patch. A source of uncertainty in our results comes from the resulting under-sampling of the dye patch. The two cross-canyon transects completed during the survey (Figure A1h, i) show that lateral distribution of the dye

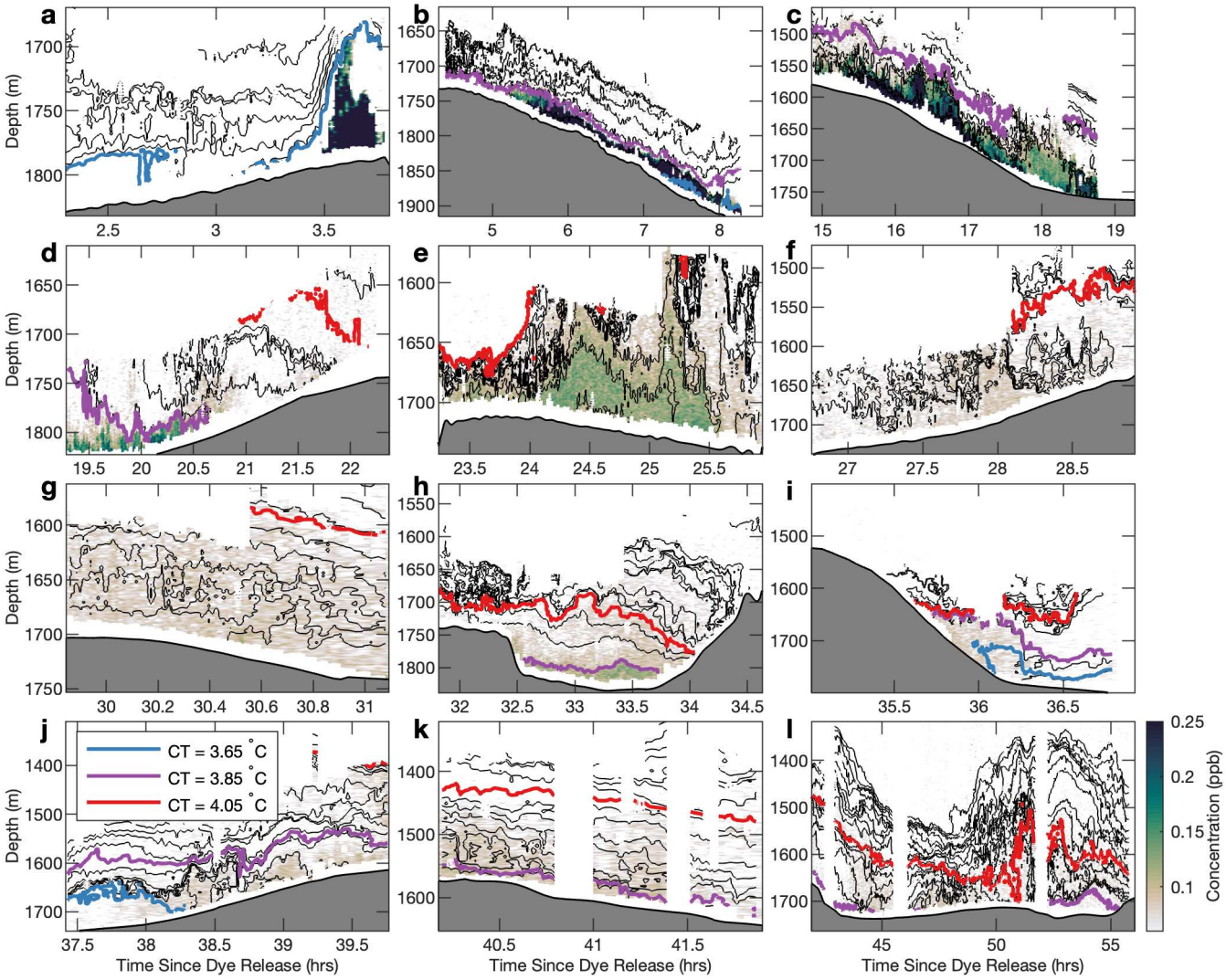

Figure A1: Every transect ((a)-(l)) of the FCTD dye survey. Dye concentration is shown in parts per billion (ppb) in colour, isotherms every 0.05°C are shown with black contours, and 3.65°C, 3.85°C and 4.05°C isotherms are contoured in blue, purple and red respectively. Note the different aspect ratio in each panel. Bathymetry is shown in grey.

varied in time or along the length of the patch. During the first cross-canyon transect, the dye was spread fairly uniformly across the canyon width; however, in the second transect, the dye was banked on the northeast side of the canyon. Thus, along-canyon transects, which focused on the canyon axis, may at times have sampled through only the edge of the patch. With only the velocity measurements from MP1 (down-canyon of the dye for most of the experiment), it is difficult to estimate where in the cross-canyon direction the dye patch might have been. Along-canyon transects may have only sampled the front or back edge or a small section of the patch at times, particularly during later transects when the dye patch was large. Based on dye measurements from MP1 (Figure 2) we know the entire patch was ∼4 km long at 20 hours after the release, and since we saw dye for the duration of the 12 hour

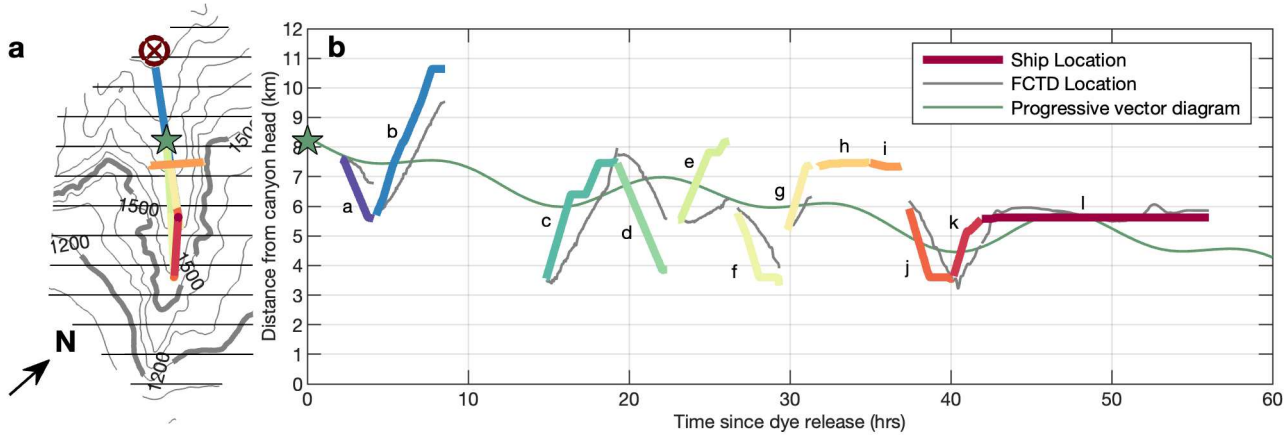

Figure A2: (a) Map of the canyon with bathymetry contoured in grey. Horizontal lines mark distance along the canyon in kilometers. Coloured lines correspond to the ship's location for each transect. MP1 location is marked by the red cross and the location of the dye release is marked by the green star. Arrow indicates the direction of north. (b) Distance along the canyon of each transect over time is shown with coloured lines, which correspond to those in panel (a) and letter labels correspond to panels in Figure A1. Thin grey lines show the approximate location of the FCTD at that time based on measured bottom depth. The green line shows integrated velocity from the MP1 mooring, with a starting position at the dye release location (green star) as an estimate of the along-canyon position of the dye patch.

time series (Figure A1l), we know the patch was longer than one excursion length of the semi-diurnal tide (∼4 km) by the end of the record. Later along-canyon transects were all shorter than this (Figure A2). To investigate the effect of under-sampling on estimates of the centre of mass, we sub-sampled the cross-canyon transects (Figure A1h, i), the longest along-canyon transects (Figure A1a, c) and the time series (Figure A1l). For each of these, subsets of 10 profiles were taken to estimate the variability in the centre of mass. Results are shown in Figure A3. The effect of sub-sampling varies depending on the transect with an average standard deviation of 0.01 kg m^{-3}.

Another artefact of our sampling was due to the phase of the tide. For example, during the second transect (Figure A1b) we sampled the dye in a down-canyon direction as the dye itself was moving down-canyon, causing the patch to appear spread over a larger extent than it actually was. Although this makes interpreting the along-canyon movement of the dye patch difficult, over-sampling should not impact the estimates of the centre of mass.

Typically, long-term chemical tracer release surveys are designed to provide information on the three-dimensional spread of the tracer. Observations are often objectively mapped to higher resolution grids[5]. These maps provide an estimate of the fraction of tracer found. Doing such an inventory is difficult given the two-dimensional nature of our sampling pattern. However, since the focus of this study is the

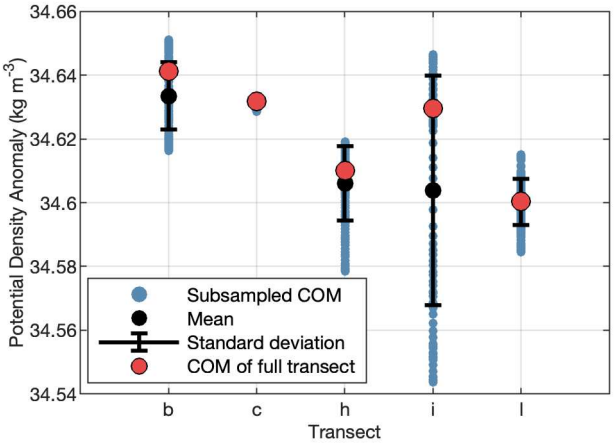

Figure A3: Range in the centre of mass for 10 profile subsections of transects b,c,h,i and l (corresponding to panels in Figure A1). Blue dots indicate the centre of mass (COM) for each subsection, the mean of these is marked by black dots and the standard deviation around this mean is indicated by error bars. COM of the entire transect is shown in red.

first rather than the second moment of the tracer, the results are less impacted by outliers.

Calculations

Centre of mass

For a dye or tracer of concentration C, the tracer-weighted average operator is defined as

$$\bar{(\cdot)} = \frac{\int\int\int (\cdot)\, C dx dy dz}{\int\int\int C dx dy dz}. \tag{A1}$$

Here, we use the first moment of the tracer weighted average of the potential density anomaly ($\overline{\sigma_\theta}$), which represents the centre of mass of the dye in density space, to describe the location of the dye patch[6;7]. Ideally, the integral is performed on the full extent of the three-dimensional dye patch. In practice, however, we are limited to the spatial information of the survey. The integrals were estimated as sums in the vertical and along-transect directions for each transect through the dye patch.

Upwelling rate

Given the first density moment, dye-weighted diapycnal velocity is given by $w_{dye} = -\frac{\partial_t \overline{\sigma_\theta}}{|\nabla \overline{\sigma_\theta}|}$ [7]. Because mixing acts on dye gradients as well as density gradients, the dye-weighted diapycnal velocity yields twice the dye-weighted density velocity, $\partial_t \overline{\sigma_\theta} = 2\overline{\dot{\sigma}_\theta}$, where $\mathrm{D}\sigma_\theta/\mathrm{D}t = \dot{\sigma}_\theta$ is the material derivative of

the potential density anomaly[7]. A total of 12 transects were completed over the 3 days before dye concentrations became too low to detect. The slope of a weighted linear regression is used to estimate the evolution of dye's centre of mass over time ($\partial_t \overline{\sigma_\theta}$; Figure A4). Weights chosen for the regression were $\mathcal{W} = \frac{n s_i^{-2}}{\sum_{i=1}^{n} s_i^{-2}}$ where s_i are standard deviations of dye weighted density for each transect $i = 1, \ldots, n$ and $n = 12$. Linear regression, with $\mathbf{R}^2 = 0.852$, yields $\partial_t \overline{\sigma_\theta} = -1.4 \times 10^{-3} \pm 0.2 \times 10^{-3}$ kg m-3 day^{-1} where the error is given by the standard error of the slope of the fit. We approximate the density gradient with its vertical component ($\overline{\partial_z \sigma_\theta}$). Here, the horizontal gradient of the density is several orders of magnitude smaller than the vertical component and therefore has a negligible impact on the vertical velocity. We calculate the tracer-averaged vertical density gradient for each transect and then use the weighted average over all the transects. The weights are equivalent to $\mathcal{W}$, but are a function of the standard deviations of the dye weighted density gradient. The density gradient used for the calculation of w_{dye} is then $\overline{\partial_z \sigma_\theta} = 1.4 \times 10^{-4} \pm 0.3 \times 10^{-4}$ kg m^{-4}. This gives an upwelling velocity of 250 ± 75 m day^{-1}, assuming that errors associated with the time rate of change of the centre of mass and the centre of mass of the vertical gradient are independent. Temporal and spatial density gradients in this location are not independent due to the strong influence of the tide on the stratification, however quantifying this effect on the centre of mass is difficult.

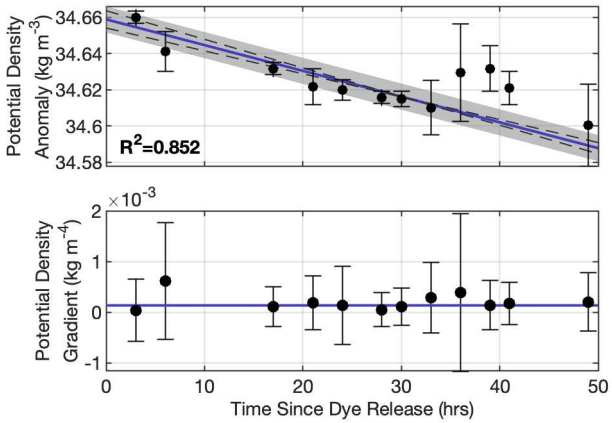

Figure A4: (a) Weighed linear regression (solid blue line) of the centres of mass in potential density anomaly space (black circles). Error bars show standard deviations of dye weighted density for each transect. The residual standard error of the fit is denoted by the shaded region. Dashed lines show the fits given the standard error on the slope and intercept. The coefficient of determination $\mathbf{R}^2$ for the fit is 0.852. (b) Centres of mass in potential density anomaly gradient space (black circles) and standard deviation for each transect (error bars). The solid blue line shows the weighted average of the centres of mass. The standard error of the average is smaller than the line width.

Hypsometry

Diapycnal upwelling due to hypsometry (w_{hyp}) within the canyon can be estimated as

$$w_{hyp} = \frac{\Gamma}{\overline{N}^2 \ell_y} \frac{\partial \left(\langle \varepsilon \rangle \ell_y \right)}{\partial z} \cong \frac{\Gamma \langle \varepsilon \rangle}{\overline{N}^2 \ell_y} \frac{\partial \ell_y}{\partial z} \cong \frac{\Gamma \langle \varepsilon \rangle}{\overline{N}^2 h}, \tag{A2}$$

where Γ is the mixing coefficient and assumed to have a constant value of 0.2[8] and ℓ_y the canyon width assumed to linearly depend on height above canyon axis h[9]. We use average values of dissipation rate of turbulent kinetic energy ϵ and stratification N^2 collected from 12 microstructure time-series stations at various locations along the canyon each spanning at least one tidal cycle (not shown). Given an average stratification of 3×10^{-6} s^{-2} and a constant dissipation rate of 5×10^{-8} W kg^{-1} within 50 m of the bottom, the upwelling velocity due to hypsometry is 5 m day^{-1}. This is 50 times smaller than the dye-measured upwelling, therefore hypsometry alone cannot explain the observations.

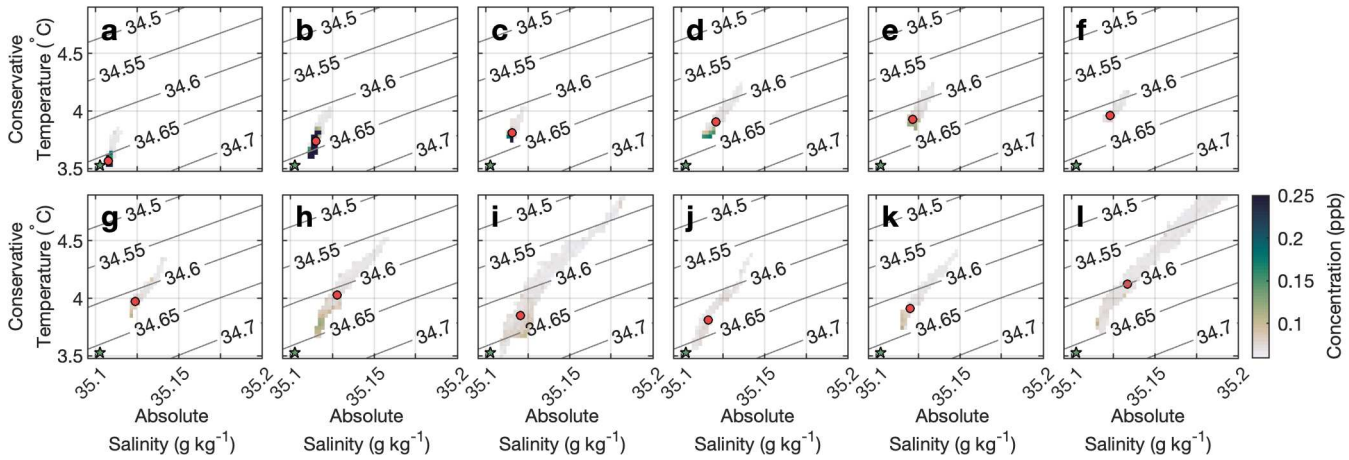

Figure A5: Binned dye concentration in conservative temperature-absolute salinity space for each transect ((a)-(l)) with contours of potential density anomaly. First tracer-weighted density moment is marked with the red circle. Potential density anomaly of the dye at the time of release is marked with the green star.

Data Availability

The mooring, Fast CTD and multibeam bathymetry data are available on request from the corresponding author. The GEBCO global bathymetry product is available at: https://www.gebco.net/data_and_products/gridded_bathymetry_data/.

Code Availability

The MATLAB (R2023b) code for data processing and generation of figures in the article are available on request from the corresponding author. The MATLAB Gibbs-SeaWater (GSW) Oceanographic Toolbox for TEOS-10 (v3.06) is available at: https://www.teos-10.org/software.htm#1.

References

[1] Naveira Garabato, A. C. 2021 RRS Discovery Cruise DY132, 19 June 2021 - 29 July 2021, Bottom Boundary Layer Turbulence and Abyssal Recipes (BLT). *National Oceanography Centre Cruise Report*, 2021.

[2] Klymak, J. M., Pinkel, R., and Rainville, L. Direct breaking of the internal tide near topography: Kaena Ridge, Hawaii. *J. Phys. Oceanogr.*, 38:380–399, 2008. doi: 10.1175/2007JPO3728.1.

[3] Alford, M. and Pinkel, R. Patterns of turbulent and double-diffusive phenomena: Observations from a rapid-profiling microconductivity probe. *J. Phys. Oceanogr.*, 30(5):833–854, 2000. doi: 10.1175/1520-0485(2000)030<0833:POTADD>2.0.CO;2.

[4] Le Boyer, A., Alford, M. H., Couto, N., Goldin, M., Lastuka, S., Goheen, S., Nguyen, S., Lucas, A. J., and Hennon, T. D. Modular, Flexible, Low-Cost Microstructure Measurements: The Epsilometer. *J. Atmos. Ocean. Tech.*, 38(3):657–668, March 2021. ISSN 0739-0572. doi: 10.1175/JTECH-D-20-0116.1.

[5] Ledwell, J. R., Watson, A. J., and Law, C. S. Mixing of a tracer in the pycnocline. *J. Geophys. Res.*, 103:21499–21529, 1998. doi: 10.1029/98JC01738.

[6] Holmes, R. M., de Lavergne, C., and McDougall, T. J. Tracer transport within abyssal mixing layers. *J. Phys. Oceanogr.*, 49(10):2669–2695, 2019. doi: 10.1175/JPO-D-19-0006.1.

[7] Ruan, X. and Ferrari, R. Diagnosing Diapycnal Mixing from Passive Tracers. *J. Phys. Oceanog.*, 51 (3):757–767, March 2021. ISSN 0022-3670. doi: 10.1175/JPO-D-20-0194.1.

[8] Osborn, T. R. Estimates of the Local Rate of Vertical Diffusion from Dissipation Measurements. *J. Phys. Oceanogr.*, 10(1):83–89, 1980. doi: 10.1175/1520-0485(1980)010<0083:EOTLRO>2.0.CO;2.

[9] Kunze, E., MacKay, C., McPhee-Shaw, E. E., Morrice, K., Girton, J. B., and Terker, S. R. Turbulent Mixing and Exchange with Interior Waters on Sloping Boundaries. *J. Phys. Oceanogr.*, 42(6):910–927, June 2012. ISSN 0022-3670. doi: 10.1175/JPO-D-11-075.1.

Acknowledgements

We thank the captain and crew of *RRS Discovery*, the National Marine Facilities technicians for assistance during the experiment and the engineers of the Multiscale Ocean Dynamics group for their assistance and design and fabrication of the instrumentation. This work was funded by the Natural Environment Research Council (grant NE/S001433/1) and the National Science Foundation (grant OCE-1756264).

Author Contributions

B.L.W.C. performed analyses, produced figures and wrote the manuscript with feedback and suggestions from all authors. M.H.A. conceived the dye study and designed the survey plan. A.N.G., G.V., K.P., M.J.M., H.M., C.P.S., A.L.B, N.C., B.L.W.C. and R.F. contributed to the design and execution of the experiment. M.J.M. and H.F.M. performed the dye release.

Competing Interest Declaration

The authors declare no competing interests.

Additional Information

Correspondence and requests for materials should be addressed to Bethan L. Wynne-Cattanach (bwynneca@ucsd.edu).